CHAPTER SEVEN
Advective Diffusion of Air Bubbles in Turbulent Water Flows

Hubert Chanson
Professor in Civil Engineering, The University of Queensland, Brisbane QLD 4072, Australia

7.1 INTRODUCTION

The exchange of air between the atmosphere and flowing water is usually called air entrainment, air bubble entrainment or self-aeration. The continuous exchange between air and water is most important for the biological and chemical equilibrium on our planet. For example, the air-water mass transfer at the surface of the oceans regulates the composition of the atmosphere. The aeration process drives the exchange of nitrogen, oxygen and carbon dioxide between the atmosphere and the sea, in particular the dissolution of carbon dioxide into the oceans and the release of supersaturated oxygen to the atmosphere. Another form of flow aeration is the entrainment of un-dissolved air bubbles at the air-water free-surface. Air bubble entrainment is observed in chemical, coastal, hydraulic, mechanical and nuclear engineering applications. In Nature, air bubble entrainment is observed at waterfalls, in mountain streams and river rapids, and in breaking waves on the ocean surface. The resulting "white waters" provide some spectacular effects (Fig. 7.7.1 to 7.4). Figure 7.7.1 illustrates the air bubble entrainment at a 83 m high waterfall with a lot of splashing and spray generated at nappe impact. Figure 7.7.2 shows some air entrainment in a hydraulic jump downstream of a spillway, and Figure 7.7.3 presents some air bubble entrainment at a plunging breaking wave. Figure 7.7.4 highlights the free-surface aeration downstream of the Three Gorges dam that may be seen from space (Fig. 7.7.4B).

Herein we define air bubble entrainment as the entrainment or entrapment of un-dissolved air bubbles and air pockets that are advected within the flowing waters. The term air bubble is used broadly to describe a volume of air surrounded continuously or not by some liquid and encompassed within some air-water interface(s). The resulting air-water mixture consists of both air packets within water and water droplets surrounded by air, and the flow structure may be quite complicated.

Further the entrainment of air bubbles may be localised at a flow discontinuity or continuous along an air-water free-surface : i.e., singular or interfacial aeration respectively. Examples of singular aeration include the air bubble entrainment by a vertical plunging jet. Air bubbles are entrained locally at the intersection of the impinging water jet with the receiving body of water. The impingement perimeter is a source of both vorticity and air bubbles. Interfacial aeration is defined as the air bubble entrainment process along an air-water interface, usually parallel to the flow direction. It is observed in spillway chute flows and in high-velocity water jets discharging into air.

After a review of the basic mechanisms of air bubble entrainment in turbulent water flows, it will be shown that the void fraction distributions may be modelled by some analytical solutions of the advective diffusion equation for air bubbles. Later the micro-structure of the air-water flow will be discussed and it will be argued that the interactions between entrained air bubbles and turbulence remain a key challenge.

Figure 7.7.1. Air bubble entrainment at a water fall - Chute Montmorency, Québec, Canada on 6 June 2004 (Fall height : 83 m) - Left: general view from downstream. Right: details of the free-surface (shutter speed: 1/1,000 s).

Figure 7.7.2. Air bubble entrainment in a hydraulic jump at the downstream end of a spillway chute - Chain Lakes dam spillway, Southern Alberta, Canada, June 2005 (Courtesy of John Rémi) - Looking downstream, with a discharge of about 300 m^3/s - Note the "brownish" dark colour of the flow caused by the suspended load and the "white" waters downstream of the hydraulic jump highlighting the air bubble detrainment.

Figure 7.7.3. Air entrainment at wave breaking - Anse des Blancs, Le Conquet, France on 19 April 2004 during early ebb tide (Shutter speed 1/200 s).

(A). Bottom outlet operation on 20 October 2004 - Q = 1700 m^3/s per jet, V = 35 m/s (Shutter speed 1/1,000 s).

(B) "White waters" created by the outlets viewed from space on 14 May 2006 - NASA image created by Jesse Allen, Earth Observatory, using ASTER data made available by NASA/GSFC/MITI/ERSDAC/JAROS, and U.S./Japan ASTER Science Team

Figure 7.7.4. Free-surface aeration by interfacial aeration and plunging jet motion at the Three Gorges dam, central Yangtze river (China).

7.2 FUNDAMENTAL PROCESSES

7.2.1 Inception of air bubble entrainment

The inception of air bubble entrainment characterises the flow conditions at which some bubble entrainment starts. Historically the inception conditions were expressed in terms of a time-averaged velocity. It was often assumed that air entrainment occurs when the flow velocity exceeds an onset velocity V_e of about 1 m/s. The

approach is approximate and it does not account for the complexity of the flow nor the turbulence properties. More detailed studies linked the onset of air entrainment with a characteristic level of normal Reynolds stress(es) next to the free-surface. For example, Ervine an Falvey (1987) and Chanson (1993) for interfacial aeration, Cummings and Chanson (1999) for plunging jet aeration, Brocchini and Peregrine (2001). Although present knowledge remains empirical and often superficial, it is thought that the inception of air entrainment may be better described in terms of tangential Reynolds stresses.

In turbulent shear flows, the air bubble entrainment is caused by the turbulence acting next to the air-water interface. Through this interface, air is continuously being trapped and released, and the resulting air-water mixture may extend to the entire flow. Air bubble entrainment occurs when the turbulent shear stress is large enough to overcome both surface tension and buoyancy effects (if any). Experimental evidences showed that the free-surface of turbulent flows exhibits some surface "undulations" with a fine-grained turbulent structure and larger underlying eddies. Since the turbulent energy is high in small eddy lengths close to the free surface, air bubble entrainment may result from the action of high intensity turbulent shear close to the air-water interface.

Free-surface breakup and bubble entrainment will take place when the turbulent shear stress is greater than the surface tension force per unit area resisting the surface breakup. That is :

$$\left|\rho_w * v_i * v_j\right| > \sigma * \frac{\pi * (r_1 + r_2)}{A} \qquad \text{inception of air entrainment (1)}$$

where ρ_W is the water density, v is the turbulent velocity fluctuation, (i, j) is the directional tensor (i, j = x, y, z), σ is the surface tension between air and water, $\pi*(r_1+r_2)$ is the perimeter along which surface tension acts, r_1 and r_2 are the two principal radii of curvature of the free surface deformation, and A is surface deformation area. Equation (1) gives a criterion for the onset of free-surface aeration in terms of the magnitude of the instantaneous tangential Reynolds stress, the air/water physical properties and the free-surface deformation properties. Simply air bubbles cannot be entrained across the free-surface until there is sufficient tangential shear relative to the surface tension force per unit area.

Considering a two-dimensional flow for which the vortical structures next to the free-surface have axes predominantly perpendicular to the flow direction, the entrained bubbles may be schematised by cylinders of radius r (Fig. 7.5). Equation (1) may be simplified into:

$$\left|\rho_w * v_i * v_j\right| > \frac{\sigma}{\pi * r} \qquad \text{cylindrical bubbles (2a)}$$

where x and y are the streamwise and normal directions respectively. For a three-dimensional flow with quasi-isotropic turbulence, the smallest interfacial area per unit volume of air is the sphere (radius r), and Equation (1) gives :

$$\left|\rho_w * v_i * v_j\right| > \frac{\sigma}{2 * \pi * r} \qquad \text{spherical bubbles (2b)}$$

Equation (2) shows that the inception of air bubble entrainment takes place in the form of relatively large bubbles. But the largest bubbles will be detrained by buoyancy and this yields some preferential sizes of entrained bubbles, observed to be about 1 to 100 mm in prototype turbulent flows (e.g. Cain 1978, Chanson 1993,1997).

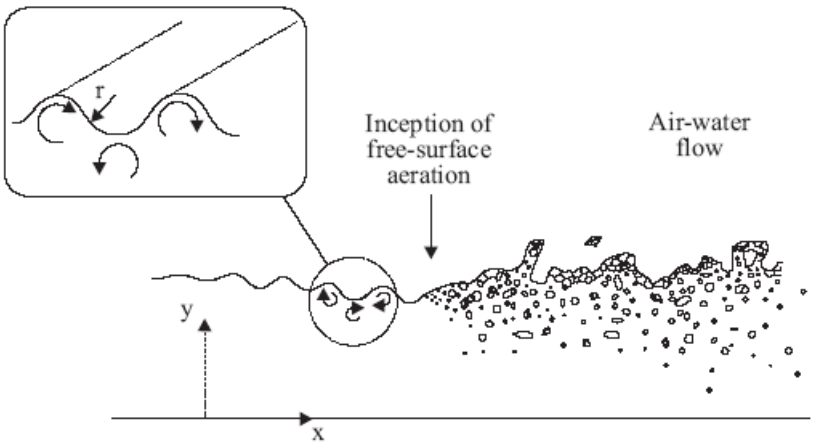

Figure 7.7.5. Inception of free-surface aeration in a two-dimensional flow.

7.2.2 Bubble breakup

The size of entrained air bubbles in turbulent shear flows is an important parameter affecting the interactions between turbulence and air bubbles. Next to the entrainment point, a region of strong mixing and momentum losses exists in which the entrained air is broken into small bubbles while being diffused within the air-water flow.

At equilibrium, the maximum bubble size in shear flows may be estimated by the balance between the surface tension force and the inertial force caused by the velocity changes over distances of the order of the bubble size. Some simple dimensional analysis yielded a criterion for bubble breakup (Hinze 1955). The result is however limited to some equilibrium situations and it is often not applicable (Chanson 1997, pp. 224-229).

In air-water flows, experimental observations of air bubbles showed that the bubble sizes are larger than the Kolmogorov microscale and smaller than the turbulent macroscale. These observations suggested that the length scale of the eddies responsible for breaking up the bubbles is close to the bubble size. Larger eddies advect the bubbles while eddies with length-scales substantially smaller than the bubble size do not have the necessary energy to break up air bubbles.

In turbulent flows, the bubble break-up occurs when the tangential shear stress is greater than the capillary force per unit area. For a spherical bubble, it yields a condition for bubble breakup :

$$\left|\rho_w * v_i * v_j\right| > \frac{\sigma}{\pi * d_{ab}} \qquad \text{spherical bubble (3a)}$$

where d_{ab} is the bubble diameter. Equation (3a) holds for a spherical bubble and the left handside term is the magnitude of the instantaneous tangential Reynolds stress. More generally, for an elongated spheroid, bubble breakup takes place for :

$$\left|\rho_w * v_i * v_j\right| > \sigma * \frac{\pi * (r_1 + r_2)}{2 * \pi * r_1 * \left(r_1 + r_2 * \frac{\text{Arc}\sin\left(\sqrt{1 - \frac{r_1^2}{r_2^2}}\right)}{\sqrt{1 - \frac{r_1^2}{r_2^2}}} \right)}$$

elongated spheroid (3b)

where r_1 and r_2 are the equatorial and polar radii of the ellipsoid respectively with $r_2 > r_1$. Equation (3b) implies that some turbulence anisotropy (e.g. v_x, $v_y >> v_z$) must induce some preferential bubble shapes.

7.3 ADVECTIVE DIFFUSION OF AIR BUBBLES. BASIC EQUATIONS.

7.3.1 Presentation

Turbulent flows are characterised by a substantial amount of air-water mixing at the interfaces. Once entrained, the air bubbles are diffused through the flow while they are advected downstream. Herein their transport by advection and diffusion are assumed two separate additive processes; and the theory of superposition is applicable.

In the bubbly flow region, the air bubble diffusion transfer rate in the direction normal to the advective direction varies directly as the negative gradient of concentration. The scalar is the entrained air and its concentration is called the void fraction C defined as the volume of air per unit volume of air and water. Assuming a steady, quasi-one-dimensional flow, and for a small control volume, the continuity equation for air in the air-water flow is:

$$\text{div}(C * \vec{V}) = \text{div}\,(D_t * \vec{\text{grad}}\, C - C * \vec{u_r}) \quad (4)$$

where C is the void fraction, $\vec{V}$ is the advective velocity vector, D_t is the air bubble turbulent diffusivity and $\vec{u_r}$ is the bubble rise velocity vector that takes into account the effects of buoyancy. Equation (4) implies a constant air density, neglects compressibility effects, and is valid for a steady flow situation.

Equation (4) is called the advective diffusion equation. It characterises the air volume flux from a region of high void fraction to one of smaller air concentration. The first term (C*V) is the advective flux while the right handside term is the diffusive flux. The latter includes the combined effects of transverse diffusion and buoyancy. Equation (4) may be solved analytically for a number of basic boundary conditions. Mathematical solutions of the diffusion equation were addressed in two classical references (Carslaw and Jaeger 1959, Crank 1956). Since Equation (4) is linear, the theory of superposition may be used to build up solutions with more complex problems and boundary conditions. Its application to air-water flows was discussed by Wood (1984,1991) and Chanson (1988,1997).

7.3.2 Buoyancy effects on submerged air bubbles

When air bubbles are submerged in a liquid, a net upward force is exerted on each bubble. That is, the buoyancy force which is the vertical resultant of the pressure forces acting on the bubble. The buoyant force equals the weight of displaced liquid.

The effects of buoyancy on a submerged air bubble may be expressed in terms of the bubble rise velocity u_r. For a single bubble rising in a fluid at rest and in a steady state, the motion equation of the rising bubble yields an exact balance between the buoyant force (upwards), the drag force (downwards) and the weight force (downwards). The expression of the buoyant force may be derived from the integration of the pressure field around the bubble and it is directly proportional to minus the pressure gradient $\partial P/\partial z$ where P is the pressure and z is the vertical axis positive upwards. In a non-hydrostatic pressure gradient, the rise velocity may be estimated to a first approximation as:

$$u_r = \pm (u_r)_{Hyd} * \sqrt{\frac{\left|\frac{\partial P}{\partial z}\right|}{\rho_w * g}} \quad (5)$$

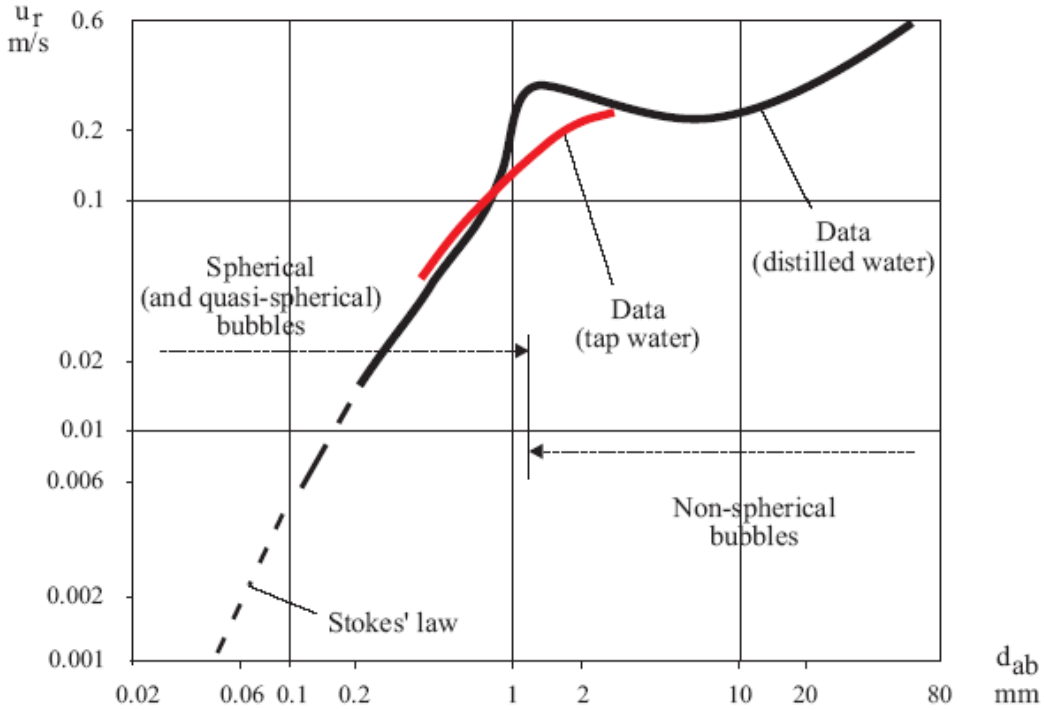

Figure 7.6. Bubble rise velocity in still water.

where $(u_r)_{Hyd}$ is the bubble rise velocity in a hydrostatic pressure gradient (Fig. 7.6), ρ_w is the liquid density, herein water, and z is the vertical direction positive upwards. The sign of the rise velocity u_r depends on the sign of $\partial P/\partial z$. For $\partial P/\partial z < 0$, u_r is positive. Experimental results of bubble rise velocity in still water are reported in Figure 7.6. Relevant references include Haberman and Morton (1954) and Comolet (1979a,b).

7.3.3 A simple application

Let us consider a two-dimensional steady open channel flow down a steep chute (Fig. 7.7). The advective diffusion equation becomes :

$$\frac{\partial}{\partial x}(V_x * C) + \frac{\partial}{\partial y}(V_y * C) = \frac{\partial}{\partial x}\left(D_t * \frac{\partial C}{\partial x}\right) + \frac{\partial}{\partial y}\left(D_t * \frac{\partial C}{\partial y}\right)$$
$$- \frac{\partial}{\partial x}(- u_r * \sin\theta * C) - \frac{\partial}{\partial y}(u_r * \cos\theta * C) \qquad (6)$$

where θ is the angle between the horizontal and the channel invert, x is the streamwise direction and y is the transverse direction (Fig. 7.7). In the uniform equilibrium flow region, the gravity force component in the flow direction is counterbalanced exactly by the friction and drag force resultant. Hence $\partial/\partial x = 0$ and $V_y = 0$. Equation (6) yields :

$$0 = \frac{\partial}{\partial y}\left(D_t * \frac{\partial C}{\partial y}\right) - \cos\theta * \frac{\partial}{\partial y}(u_r * C) \qquad (7)$$

where D_t is basically the diffusivity in the direction normal to the flow direction.

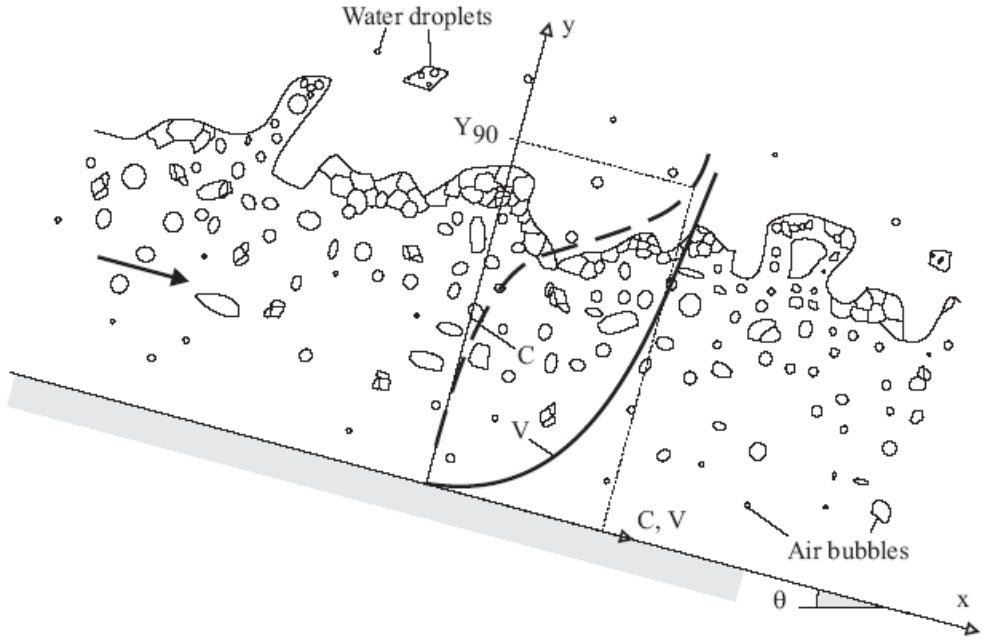

Figure 7.7. Self-aeration in a high-velocity open channel flow.

At a distance y from the invert, the fluid density is $\rho = \rho_W*(1 - C)$ where C is the local void fraction. Hence the expression of the bubble rise velocity (Eq. (5)) becomes:

$$u_r = (u_r)_{Hyd} * \sqrt{1 - C} \quad (8)$$

Equation (8) gives the rise velocity in a two-phase flow mixture of void fraction C as a function of the rise velocity in hydrostatic pressure gradient. The buoyant force is smaller in aerated waters than in clear-water. For example, a heavy object might sink faster in "white waters" because of the lesser buoyancy.

The advective diffusion equation for air bubbles may be rewritten in dimensionless terms:

$$\frac{\partial}{\partial y'}\left(D' * \frac{\partial C}{\partial y'}\right) = \frac{\partial}{\partial y'}(C * \sqrt{1 - C}) \quad (7b)$$

where $y' = y/Y_{90}$, Y_{90} is the characteristic distance where C = 0.90, $D' = D_t/((u_r)_{Hyd}*\cos\theta*Y_{90})$ is a dimensionless turbulent diffusivity and the rise velocity in hydrostatic pressure gradient $(u_r)_{Hyd}$ is assumed a constant. D' is the ratio of the air bubble diffusion coefficient to the rise velocity component normal to the flow direction time the characteristic transverse dimension of the shear flow.

A first integration of Equation (7) leads to :

$$\frac{\partial C}{\partial y'} = \frac{1}{D'} * C * \sqrt{1 - C} \quad (9)$$

Assuming a homogeneous turbulence across the flow (D' = constant), a further integration yields:

$$C = 1 - \tanh^2\left(K' - \frac{y'}{2 * D'}\right) \quad (10)$$

where K' is an integration constant and tanh(x) is the hyperbolic tangent function. The void fraction distribution (Eq. (10)) is a function of two constant parameters : the dimensionless diffusivity D' and the dimensionless constant K'. A relationship between D' and K' is deduced at the boundary condition C = 0.90 at y' = 1 :

$$K' = K^* + \frac{1}{2 * D'} \tag{11}$$

where $K^* = \tanh^{-1}(\sqrt{0.1}) = 0.32745015...$ If the diffusivity is unknown, it can deduced from the depth averaged void fraction C_{mean} defined as:

$$C_{mean} = \int_0^1 C * dy' \tag{12}$$

It yields :

$$C_{mean} = 2 * D' * \left(\tanh\left(K^* + \frac{1}{2 * D'}\right) - \tanh(K^*)\right) \tag{13}$$

7.4 ADVECTIVE DIFFUSION OF AIR BUBBLES. ANALYTICAL SOLUTIONS.

In turbulent shear flows, the air bubble entrainment processes differ substantially between singular aeration and interfacial aeration. Singular (local) air entrainment is localised at a flow discontinuity : e.g., the intersection of the impinging water jet with the receiving body of water. The air bubbles are entrained locally at the flow singularity: e.g., the toe of a hydraulic jump (Fig. 7.2). The impingement perimeter is a source of air bubbles as well as a source of vorticity. Interfacial (continuous) aeration takes place along an air-water free-surface, usually parallel to the flow direction : e.g., spillway chute flow (Fig. 7.7). Across the free-surface, air is continuously entrapped and detrained, and the entrained air bubbles are advected in regions of relatively low shear.
In the following paragraphs, some analytical solutions of Equation (4) are developed for both singular and interfacial air entrainment processes.

7.4.1 Singular aeration

7.4.1.1 Air bubble entrainment at vertical plunging jets

Considering a vertical plunging jet, air bubbles may be entrained at impingement and carried downwards below the pool free surface (Fig. 7.8). This process is called plunging jet entrainment. In chemical engineering, plunging jets are used to stir chemicals as well as to increase gas-liquid mass transfer. Plunging jet devices are used also in industrial processes (e.g. bubble flotation of minerals) while planar plunging jets are observed at dam spillways and overfall drop structures. A related flow situation is the plunging breaking wave in the ocean (Fig. 7.3).

The air bubble diffusion at a plunging liquid jet is a form of advective diffusion. For a small control volume and neglecting the buoyancy effects, the continuity equation for air bubbles becomes :

$$\text{div}(C \vec{V}) = \text{div}(D_t * \overrightarrow{\text{grad}}\, C) \tag{14}$$

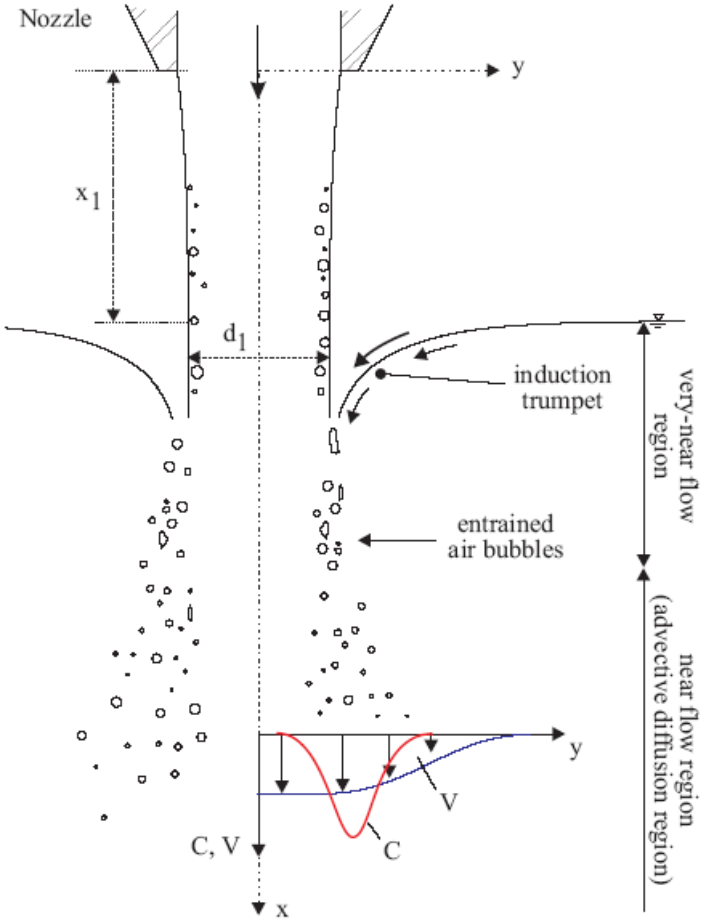

Figure 7.8. Advection of air bubbles downstream of the impingement of a vertical plunging jet.

In Equation (14), the bubble rise velocity term may be neglected because the jet velocity is much larger than the rise velocity.

For a circular plunging jet, assuming an uniform velocity distribution, for a constant diffusivity (in the radial direction) independent of the longitudinal location and for a small control volume delimited by streamlines (i.e. stream tube), Equation (14) becomes a simple advective diffusion equation:

$$\frac{V_1}{D_t} * \frac{\partial C}{\partial x} = \frac{1}{r} * \frac{\partial}{\partial y}\left(y * \frac{\partial C}{\partial y}\right) \quad (15)$$

where x is the longitudinal direction, y is the radial distance from the jet centreline, V_1 is the jet impact velocity and the diffusivity term D_t averages the effects of the turbulent diffusion and of the longitudinal velocity gradient.

The boundary conditions are : $C(x<x_1, y \leq d_1/2) = 0$ and a circular source of total strength Q_{air} at $(x\text{-}x_1=0, y=d_1/2)$ where d_1 is the jet diameter at impact (Fig. 7.8). Equation (15) can be solved analytically by applying a superposition method. The general solution of the advective diffusion equation is :

$$C = \frac{Q_{air}}{Q_w} * \frac{1}{4 * D^{\#} * \frac{x - x_1}{d_1/2}} * \exp\left(- \frac{1}{4 * D^{\#}} * \frac{\left(\frac{y}{d_1/2}\right)^2 + 1}{\frac{x - x_1}{d_1/2}} \right) * I_o\left(\frac{1}{2 * D^{\#}} * \frac{\frac{y}{d_1/2}}{\frac{x - x_1}{d_1/2}} \right)$$

Circular plunging jet (16)

where I_o is the modified Bessel function of the first kind of order zero and $D^{\#} = D_t/(V_1 * d_1/2)$.

For a two-dimensional free-falling jet, the air bubbles are entrapped at the point sources ($x=x_1$, $y=+d_1/2$) and ($x=x_1$, $y=-d_1/2$). Assuming an uniform velocity distribution, for a diffusion coefficient independent of the transverse location and for a small control volume (dx, dy) limited between two streamlines, the continuity equation (Eq. (14)) becomes a two-dimensional diffusion equation:

$$\frac{V_1}{D_t} * \frac{\partial C}{\partial x} = \frac{\partial^2 C}{\partial y^2} \tag{17}$$

where y is the distance normal to the jet centreline (Fig. 7.8). The problem can be solved by superposing the contribution of each point source. The solution of the diffusion equation is :

$$C = \frac{1}{2} * \frac{Q_{air}}{Q_w} * \frac{1}{\sqrt{4 * \pi * D^{\#} * \frac{x - x_1}{d_1}}} * \left(\exp\left(- \frac{1}{4 * D^{\#}} * \frac{\left(\frac{y}{d_1} - 1\right)^2}{\frac{x - x_1}{d_1}} \right) + \exp\left(- \frac{1}{4 * D^{\#}} * \frac{\left(\frac{y}{d_1} + 1\right)^2}{\frac{x - x_1}{d_1}} \right) \right)$$

Two-dimensional plunging jet (18)

where Q_{air} is the entrained air flow rate, Q_w is the water flow rate , d_1 is the jet thickness at impact, and $D^{\#}$ is a dimensionless diffusivity : $D^{\#} = D_t/(V_1 * d_1)$.

Discussion

Equations (16) and (18) are the exact analytical solutions of the advective diffusion of air bubbles (Eq. (4)). The two-dimensional and axi-symmetrical solutions differ because of the boundary conditions and of the integration method. Both solutions are three-dimensional solutions valid in the developing bubbly region and in the fully-aerated flow region. They were successfully compared with a range of experimental data.

7.4.1.2 Air bubble entrainment in a horizontal hydraulic jump

A hydraulic jump is the sudden transition from a supercritical flow into a slower, subcritical motion (Fig. 7.9). It is characterised by strong energy dissipation, spray and splashing and air bubble entrainment. The hydraulic jump is sometimes described as the limiting case of a horizontal supported plunging jet.

Assuming an uniform velocity distribution, for a constant diffusivity independent of the longitudinal and transverse location, Equation (14) becomes :

$$V_1 * \frac{\partial C}{\partial x} + u_r * \frac{\partial C}{\partial y} = D_t * \frac{\partial^2 C}{\partial y^2} \tag{19}$$

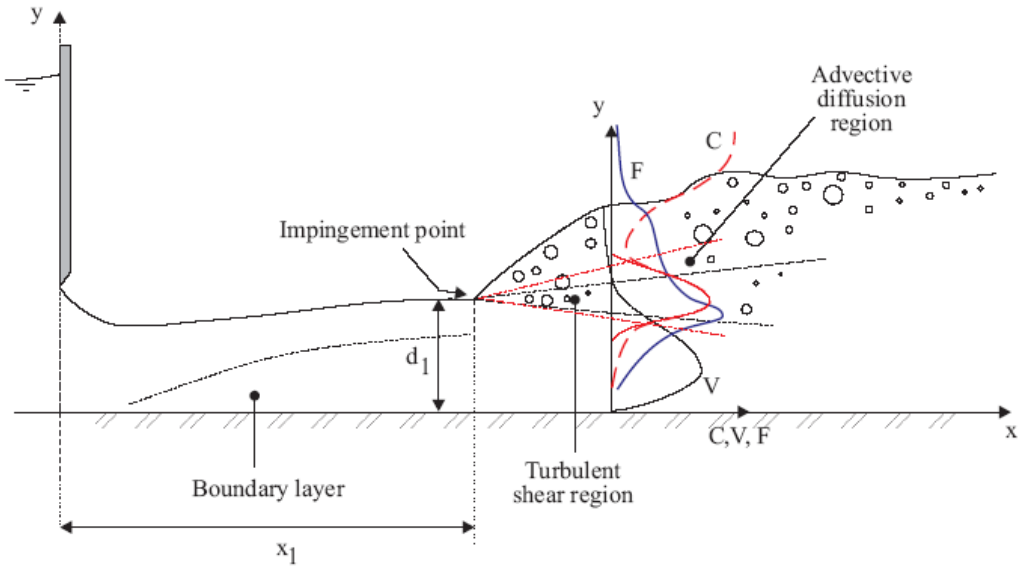

(A) Definition sketch.

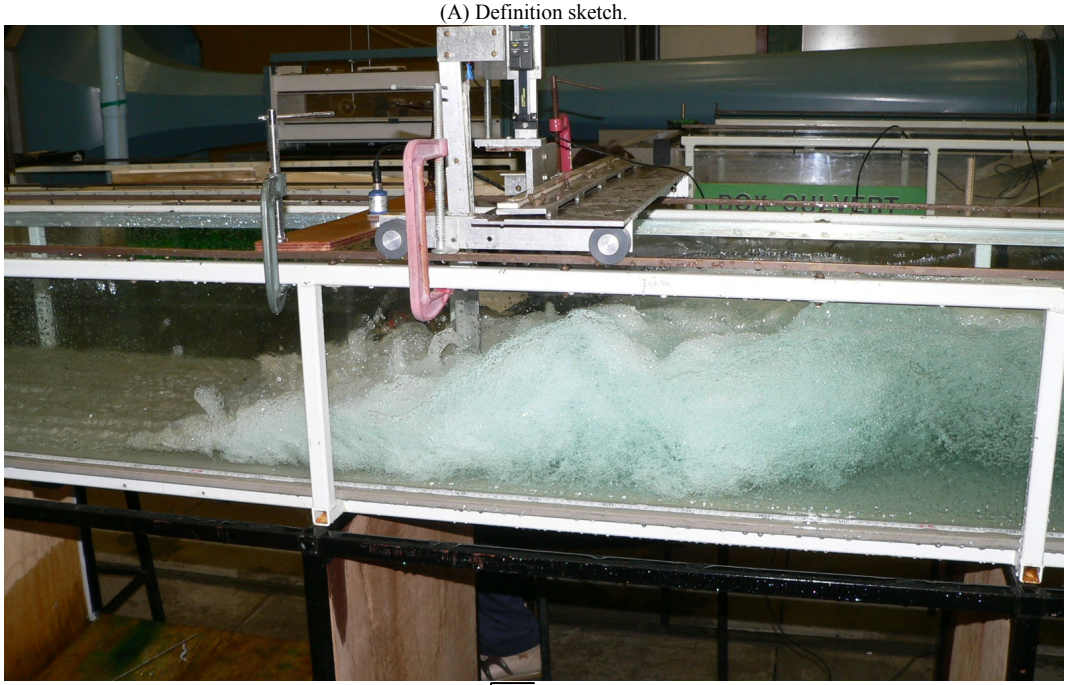

(B) Hydraulic jump in a rectangular channel ($V_1/\sqrt{g*d_1}$ = 7, $\rho_w*V_1*d_1/\mu_w$ = 8.1 E+4) - Flow from left to right.

Figure 7.9. Advection of air bubbles in a horizontal hydraulic jump.

where V_1 is the inflow velocity and the rise velocity is assumed constant. With a change of variable ($X = x - x_1 + u_r/V_1*y$) and assuming $u_r/V_1 << 1$, Equation (19) becomes a two-dimensional diffusion equation:

$$\frac{V_1}{D_t} * \frac{\partial C}{\partial X} = \frac{\partial^2 C}{\partial y^2} \tag{20}$$

In a hydraulic jump, the air bubbles are supplied by a point source located at ($X= u_r/V_1*d_1$, $y=+d_1$) and the strength of the source is Q_{air}/W where W is the channel width.

The diffusion equation can be solved by applying the method of images and assuming an infinitesimally long channel bed. It yields:

$$C = \frac{Q_{air}}{Q_w} * \frac{1}{\sqrt{4 * \pi * D^{\#} * X'}} * \left(\exp\left(- \frac{1}{4 * D^{\#}} * \frac{\left(\frac{y}{d_1} - 1\right)^2}{X'} \right) + \exp\left(- \frac{1}{4 * D^{\#}} * \frac{\left(\frac{y}{d_1} + 1\right)^2}{X'} \right) \right) \quad (21)$$

where d_1 is the inflow depth, $D^{\#}$ is a dimensionless diffusivity: $D^{\#} = D_t/(V_1*d_1)$ and :

$$X' = \frac{X}{d_1} = \frac{x - x_1}{d_1} * \left(1 + \frac{u_r}{V_1} * \frac{y}{x - x_1} \right)$$

Equation (21) is close to Equation (18) but the distribution of void fraction is shifted upwards as a consequence of some buoyancy effect. Further the definition of d_1 differs (Fig. 7.9). In practice, Equation (21) provides a good agreement with experimental data in the advective diffusion region of hydraulic jumps with partially-developed inflow conditions.

7.4.2 Interfacial aeration

7.4.2.1 Interfacial aeration in a water jet discharging into the atmosphere

High velocity turbulent water jets discharging into the atmosphere are often used in hydraulic structures to dissipate energy. Typical examples include jet flows downstream of a ski jump at the toe of a spillway, water jets issued from bottom outlets (Fig. 7.10B) and flows above a bottom aeration device along a spillway. Other applications include mixing devices in chemical plants and spray devices. High-velocity water jets are used also for fire-fighting jet cutting (e.g. coal mining), with Pelton turbines and for irrigation (Fig. 7.10C).

Considering a water jet discharging into air, the pressure distribution is quasi-uniform across the jet and the buoyancy effect is zero in most cases. For a small control volume, the advective diffusion equation for air bubbles in a steady flow is :

$$\text{div}(C \vec{V}) = \text{div}(D_t * \overrightarrow{\text{grad}}\, C) \quad (14)$$

For a circular water jet, the continuity equation for air becomes:

$$\frac{\partial}{\partial x}(C * V_1) = \frac{1}{y} * \frac{\partial}{\partial y}\left(D_t * y * \frac{\partial C}{\partial y} \right) \quad (22)$$

where x is the longitudinal direction, y is the radial direction, V_1 is the jet velocity and D_t is the turbulent diffusivity in the radial direction.

Assuming a constant diffusivity D_t in the radial direction, and after separating the variables, the void fraction :

$$C = \mathbf{u} * \exp\left(- \frac{D_t}{V_1} * \alpha_n{}^2 * x \right)$$

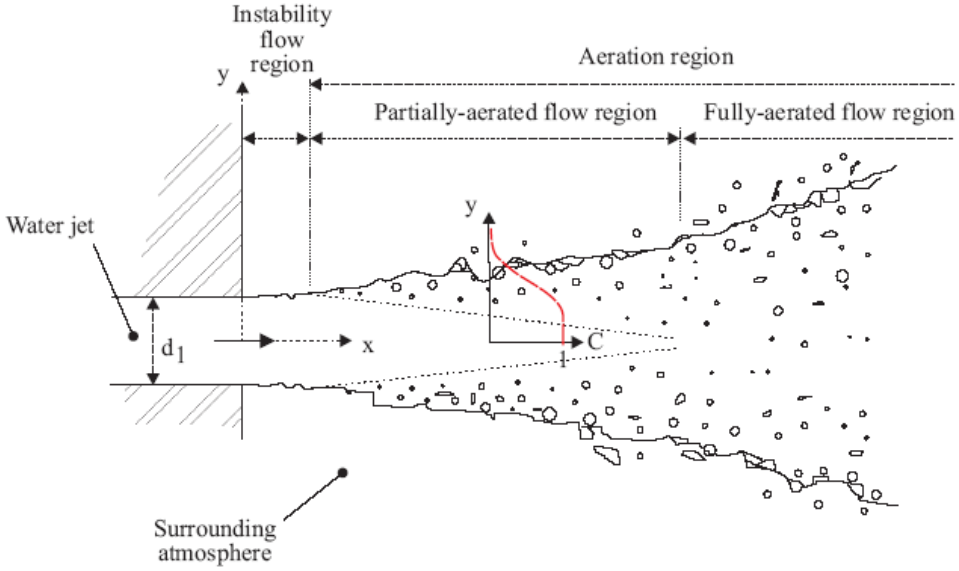

(A) Definition sketch.

(B) High-velocity water jet at Three Gorges dam - 9 m by 7 m jet, V_1 = 35 m/s, high-shutter speed (1/1,000 s).

(C) Circular water jet (irrigation water canon) - d_1 = 0.0275 m, V_1 = 22.5 m/s, high-shutter speed (1/1,000 s).

Figure 7.10. Advective dispersion of air bubbles in a turbulent water jet discharging into air.

is a solution of the continuity equation provided that u is a function of y only satisfying the Bessel's equation of order zero :

$$\frac{\partial^2 \mathbf{u}}{\partial y^2} + \frac{1}{y} * \frac{\partial \mathbf{u}}{\partial y} + \alpha_n{}^2 * \mathbf{u} = 0 \qquad (23)$$

At each position x, the diffusivity D_t is assumed a constant independent of the transverse location y. The boundary conditions are C = 0.9 at $y = Y_{90}$ for $x > 0$ and C = 0 for $x < 0$. An analytical solution is a series of Bessel functions :

$$C = 0.9 - \frac{1.8}{Y_{90}} * \sum_{n=1}^{+\infty} \frac{J_o(y*\alpha_n)}{\alpha_n * J_1(Y_{90}*\alpha_n)} * \exp\left(- \frac{D_t}{V_1} * \alpha_n{}^2 * x \right) \qquad (24)$$

where J_o is the Bessel function of the first kind of order zero, α_n is the positive root of : $J_o(Y_{90}*\alpha_n) = 0$, and J_1 is the Bessel function of the first kind of order one. Equation (24) was numerically computed by Carslaw and Jaeger (1959) for several values of the dimensionless diffusivity $D'' = D_t*x/(V_1* Y_{90}{}^2)$.

Equation (24) is valid close to and away from the jet nozzle. It is a three-dimensional solution of the diffusion equation that it is valid when the clear water core of the jet disappears and the jet becomes fully-aerated.

For a two-dimensional water jet, assuming an uniform velocity distribution, and for a constant diffusivity independent of the longitudinal and transverse location, Equation (14) becomes :

$$V_1 * \frac{\partial C}{\partial x} = D_t * \frac{\partial^2 C}{\partial y^2} \qquad (25)$$

where V_1 is the inflow depth. Equation (25) is a basic diffusion equation (Crank 1956, Carslaw and Jaeger 1959).

The boundary conditions are: $\lim(C(x>0, y\rightarrow+\infty)) = 1$ and $\lim(C(x>0, y\rightarrow-\infty)) = 1$, where the positive direction for the x- and y-axes is shown on Figure 7.10A. Note that, at the edge of the free-shear layer, the rapid change of shear stress is dominant. The effect of the removal of the bottom shear stress is to allow the fluid to accelerate. Further downstream the acceleration decreases rapidly down to zero.
The analytical solution of Equation (25) is :

$$C = \frac{1}{2} * \left(2 + \text{erf}\left(\frac{\frac{y}{d_1} - \frac{1}{2}}{2 * \sqrt{\frac{D_t}{V_1 * d_1} * \frac{x}{d_1}}} \right) + \text{erf}\left(\frac{\frac{y}{d_1} + \frac{1}{2}}{2 * \sqrt{\frac{D_t}{V_1 * d_1} * \frac{x}{d_1}}} \right) \right) \quad (26)$$

where d_1 is the jet thickness at nozzle, erf is the Gaussian error function, and the diffusivity D_t averages the effect of the turbulence on the transverse dispersion and of the longitudinal velocity gradient. The boundary conditions imply the existence of a clear-water region between the air-bubble diffusion layers in the initial jet flow region as sketched in Figure 7.10A.

The two-dimensional case may be simplified for a two-dimensional free-shear layer : e.g. an open channel flow taking off a spillway aeration device or a ski jump. The analytical solution for a free shear layer is :

$$C = \frac{1}{2} * \left(1 + \text{erf}\left(\frac{\frac{y}{d_1}}{2 * \sqrt{\frac{D_t}{V_1 * d_1} * \frac{x}{d_1}}} \right) \right) \quad (27)$$

where y = 0 at the flow singularity (i.e. nozzle edge) and y > 0 towards the atmosphere.

7.4.3 Discussion

The above expressions (Sections 7.4.1 & 7.4.2) were developed assuming a constant, uniform air bubble diffusivity. While the analytical solutions are in close agreement with experimental data (e.g. Chanson 1997, Toombes 2002, Gonzalez 2005, Murzyn et al. 2005), the distributions of turbulent diffusivity are unlikely to be uniform in complex flow situations. Two well-documented examples are the skimming flow on a stepped spillway and the flow downstream of a drop structure (Fig. 7.11).

For a two-dimensional open channel flow, the advective diffusion equation for air bubbles yields :

$$\frac{\partial}{\partial y'}\left(D' * \frac{\partial C}{\partial y'} \right) = \frac{\partial}{\partial y'}(C * \sqrt{1 - C}) \quad (7b)$$

where $y' = y/Y_{90}$, Y_{90} is the characteristic distance where C = 0.90, and $D' = D_t/((u_r)_{Hyd} * \cos\theta * Y_{90})$ is a dimensionless turbulent diffusivity that is the ratio of the air bubble diffusion coefficient to the rise velocity component normal to the flow direction time the characteristic transverse dimension of the shear flow. In a skimming flow on a stepped chute (Fig. 7.11A), the flow is extremely turbulent and the air bubble diffusivity distribution may be approximated by :

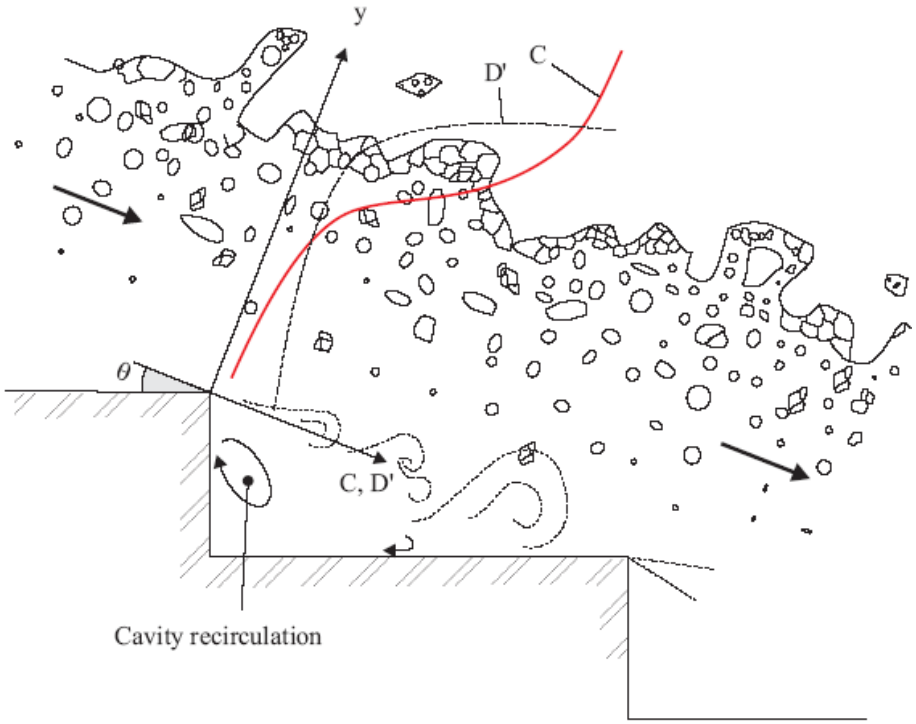

(A) Skimming flow on a stepped chute.

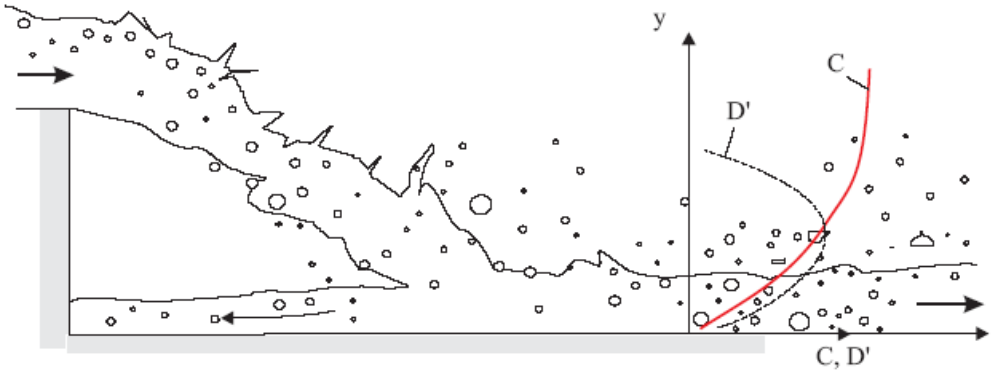

(B) Flow downstream of a nappe impact.

Figure 7.11. Advective dispersion of air bubbles in highly-turbulent open channel flows.

$$D' = \frac{D_o}{1 - 2 * \left(y' - \frac{1}{3}\right)^2} \quad (28)$$

The integration of the air bubble diffusion equation yields a S-shape void fraction profile:

$$C = 1 - \tanh^2\left(K' - \frac{y'}{2 * D_o} + \frac{\left(y' - \frac{1}{3}\right)^3}{3 * D_o}\right) \quad (29)$$

where K' is an integration constant and D_o is a function of the mean void fraction only :

$$K' = K^* + \frac{1}{2*D_o} - \frac{8}{81*D_o} \quad \text{with } K^* = 0.32745015... \quad (30)$$

$$C_{mean} = 0.7622*(1.0434 - \exp(-3.614*D_o)) \quad (31)$$

Equations (28) and (29) are sketched in Figure 7.11A. They were found to agree well with experimental measurements at step edges.

Downstream of a drop structure (Fig. 7.11B), the flow is fragmented, highly aerated and extremely turbulent. A realistic void fraction distribution model may be developed assuming a quasi-parabolic bubble diffusivity distribution :

$$D' = \frac{C * \sqrt{1 - C}}{\lambda * (K' - C)} \quad (32)$$

The integration of Equation (7b) yields :

$$C = K' * (1 - \exp(- \lambda * y')) \quad (33)$$

where K' and λ are some dimensionless functions of the mean air content only :

$$K' = \frac{0.9}{1 - \exp(-\lambda)} \quad (34)$$

$$C_{mean} = K' - \frac{0.9}{\lambda} \quad (35)$$

Equations (32) and (33) are sketched in Figure 7.11B. In practice, Equation (33) applies to highly-aerated, fragmented flows like the steady flows downstream of drop structures and spillway bottom aeration devices, and the transition flows on stepped chutes, as well as the leading edge of unsteady surges. Note that the depth-averaged air content must satisfy $C_{mean} > 0.45$.

7.5 STRUCTURE OF THE BUBBLY FLOW

In Sections 3 and 4, the advective diffusion equation for air bubbles is developed and solved in terms of the void fraction. The void fraction is a gross parameter that does not describe the air-water structures, the bubbly flow turbulence nor the interactions between entrained bubbles and turbulent shear. Herein recent experimental developments are discussed in terms of the streamwise flow structure and the air-water time and length scales.

7.5.1 Streamwise particle grouping

With modern phase-detection intrusive probes, the probe output signals provide a complete characterisation of the streamwise air-water structure at one point. Figure 7.12 illustrates the operation of such a probe. Figure 7.12B shows two probes in a bubbly flow, while Figure 7.12A presents the piercing of air bubbles by the probe sensor. Some simple signal processing yields the basic statistical moments of air and water chords as well as the probability distribution functions of the chord sizes.

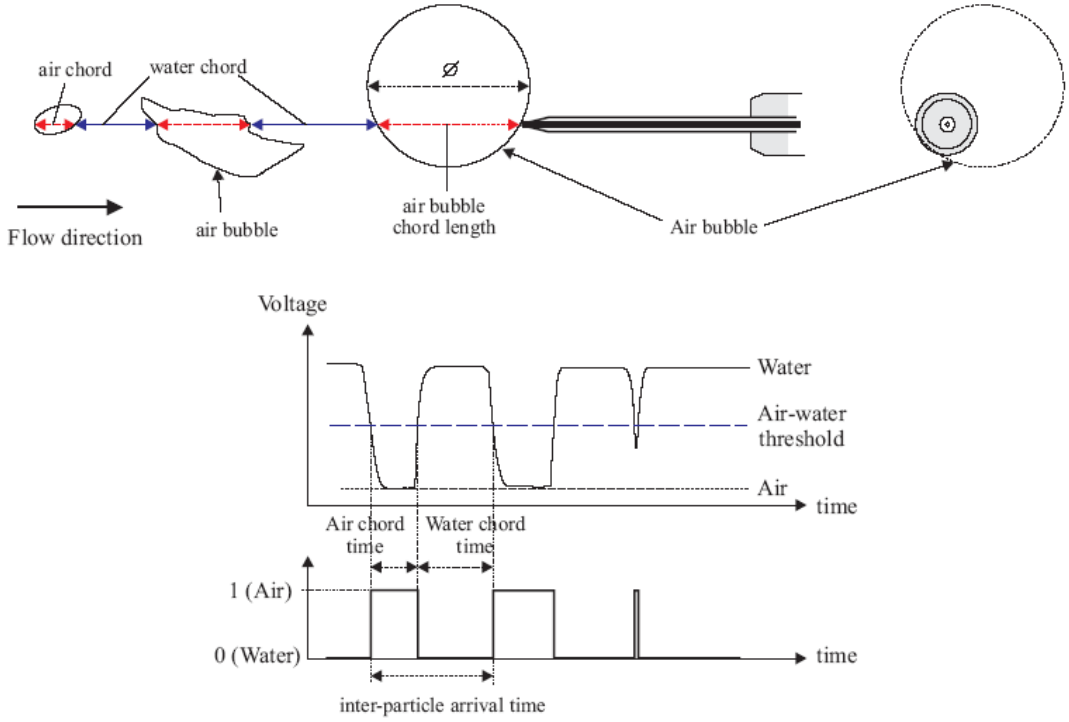

(A) Sketch of a phase-detection intrusive probe and its signal output.

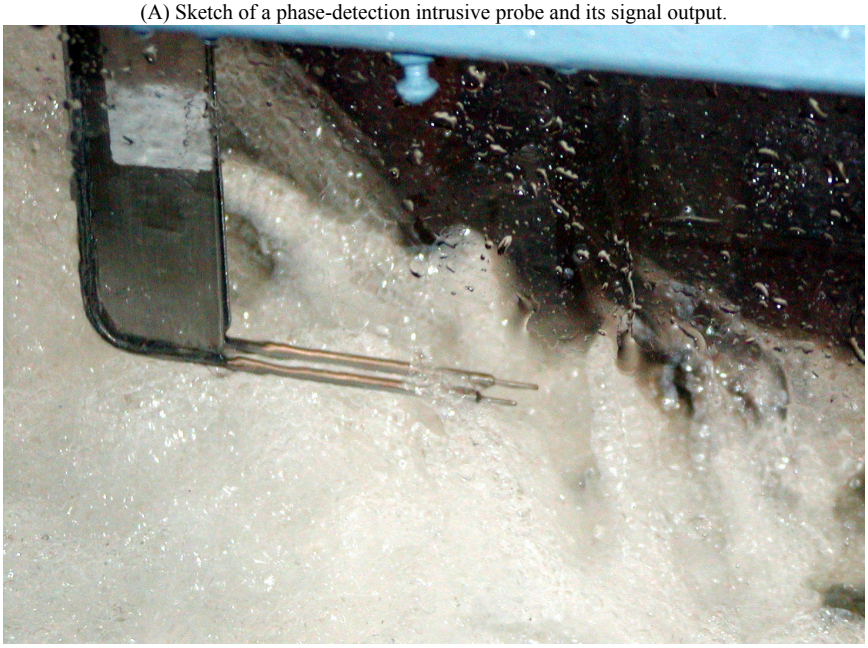

(B) Photograph of two single-tip conductivity probes side-by-side in a hydraulic jump (Fr_1 = 7.9, $\rho_w * V_1 * d_1 / \mu_w$ = 9.4 E+4) - Flow from right to left.

Figure 7.12. Phase-detection intrusive probe in turbulent air-water flows.

In turbulent shear flows, the experimental results demonstrated a broad spectrum of bubble chords. The range of bubble chord lengths extended over several orders of magnitude including at low void fractions. The distributions of bubble chords were skewed with a preponderance of small bubbles relative to the mean. The probability distribution functions of bubble chords tended to follow a log–normal and gamma distributions. Similar findings were observed in a variety of flows encompassing hydraulic jumps, plunging jets, dropshaft flows and high-velocity open channel flows.

In addition of void fraction and bubble chord distributions, some further signal processing may provide some information on the streamwise structure of the air-water flow including bubble clustering. A concentration of bubbles within some relatively short intervals of time may indicate some clustering while it may be instead the consequence of a random occurrence. The study of particle clustering events is relevant to infer whether the formation frequency responds to some particular frequencies of the flow. Figure 7.13 illustrates some occurrence of bubble pairing in the shear layer of a hydraulic jump. The binary pairing indicator is unity if the water chord time between adjacent bubbles is less than 10% of the median water chord time. The pattern of vertical lines seen in Figure 7.13 is an indication of patterns in which bubbles tend to form bubble groups.

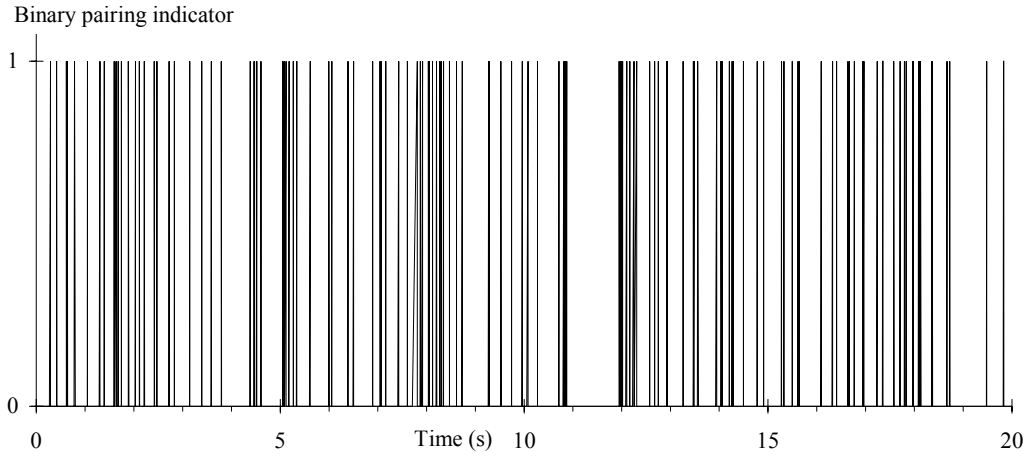

Figure 7.13. Closely spaced bubble pairs in the developing shear layer of a hydraulic jump - $Fr_1 = 8.5$, $\rho_w * V_1 * d_1 / \mu_w = 9.8$ E+4, $x\text{-}x_1 = 0.4$ m, $d_1 = 0.024$ m, $y/d_1 = 1.33$, C = 0.20, F = 158 Hz.

One method is based upon the analysis of the water chord between two adjacent air bubbles (Fig. 7.12A). If two bubbles are closer than a particular length scale, they can be considered a group of bubbles. The characteristic water length scale may be related to the water chord statistics: e.g., a bubble cluster may be defined when the water chord was less than a given percentage of the mean water chord. Another criterion may be related to the leading bubble size itself, since bubbles within that distance are in the near-wake of and may be influenced by the leading particle.

Typical results may include the percentage of bubbles in clusters, the number of clusters per second, and the average number of bubbles per cluster. Extensive experiments in open channels, hydraulic jumps and plunging jets suggested that the outcomes were little affected by the cluster criterion selection. Most results indicated that the streamwise structure of turbulent flows was characterised by about 10 to 30% of bubbles travelling as parts of a group/cluster, with a very large majority of clusters comprising of 2 bubbles only. The experimental experience suggested further that a proper cluster analysis requires a high-frequency scan rate for a relatively long scan duration. However the analysis is restricted to the streamwise distribution of bubbles and does not take into account particles travelling side by side.

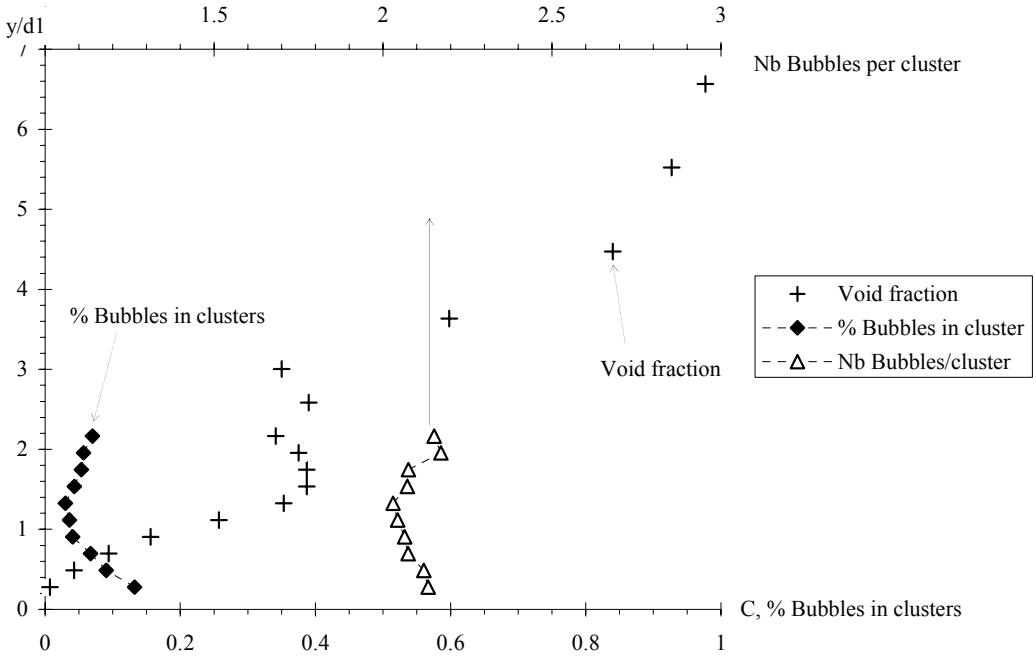

Figure 7.14. Bubble clustering in the bubbly flow region of a hydraulic jump: percentage of bubbles in clusters, average number of bubbles per cluster and void fraction - Cluster criterion : water chord time < 10% median water chord time - $Fr_1 = 8.5$, $\rho_w * V_1 * d_1 / \mu_w = 9.8$ E+4, x-$x_1 = 0.3$ m, $d_1 = 0.024$ m.

Some typical result is presented in Figure 7.14. Figure 7.14 shows the vertical distribution of the percentage of bubbles in clusters (lower horizontal axis) and average number of bubbles per cluster (upper horizontal axis) in the advective diffusion region of a hydraulic jump. The void fraction distribution is also shown for completeness. The criterion for cluster existence is a water chord less than 10% of the median water chord. For this example, about 5 to 15% of all bubbles were part of a cluster structure and the average number of bubbles per cluster was about 2.1.

For a dispersed phase, a complementary approach is based upon an inter-particle arrival time analysis. The inter-particle arrival time is defined as the time between the arrival of two consecutive bubbles recorded by a probe sensor fixed in space (Fig. 7.12A). The distribution of inter-particle arrival times provides some information on the randomness of the structure. Random dispersed flows are those whose inter-particle arrival time distributions follow inhomogeneous Poisson statistics assuming non-interacting point particles (Edwards and Marx 1995a). In other words, an ideal dispersed flow is driven by a superposition of Poisson processes of bubble sizes, and any deviation from a Poisson process indicates some unsteadiness and particle clustering.

In practice, the analysis is conducted by breaking down the air-water flow data into narrow classes of particles of comparable sizes that are expected to have the same behaviour (Edwards and Marx 1995b). A simple means consists in dividing the bubble/droplet population in terms of the air/water chord time. The inter-particle arrival time analysis may provide some information on preferential clustering for particular classes of particle sizes.

Some results in terms of inter-particle arrival time distributions are shown in Figure 7.15 for the same flow conditions and at the same cross-section as the data presented in Figure 7.14. Chi-square values are given in the figure 7.captions. Figure 7.15 presents some inter-particle arrival time results for two chord time classes of the same sample (0 to 0.5 msec. and 3 to 5 msec.). For each class of bubble sizes, a comparison between data and Poisson distribution gives some information on its randomness. For example, Figure 7.15A shows that the data for bubble chord times below 0.5 msec. did not experience a random behaviour because the experimental and theoretical distributions differed substantially in shape. The second smallest inter-particle time class (0.5-1 msec.) had a population that was 2.5 times the expected value or about 11 standard deviations too large. This indicates that there was a higher probability of having bubbles with shorter inter-particle arrival times, hence some bubble clustering occurred. Simply the smallest class of bubble chord times did not exhibit the characteristics of a random process.

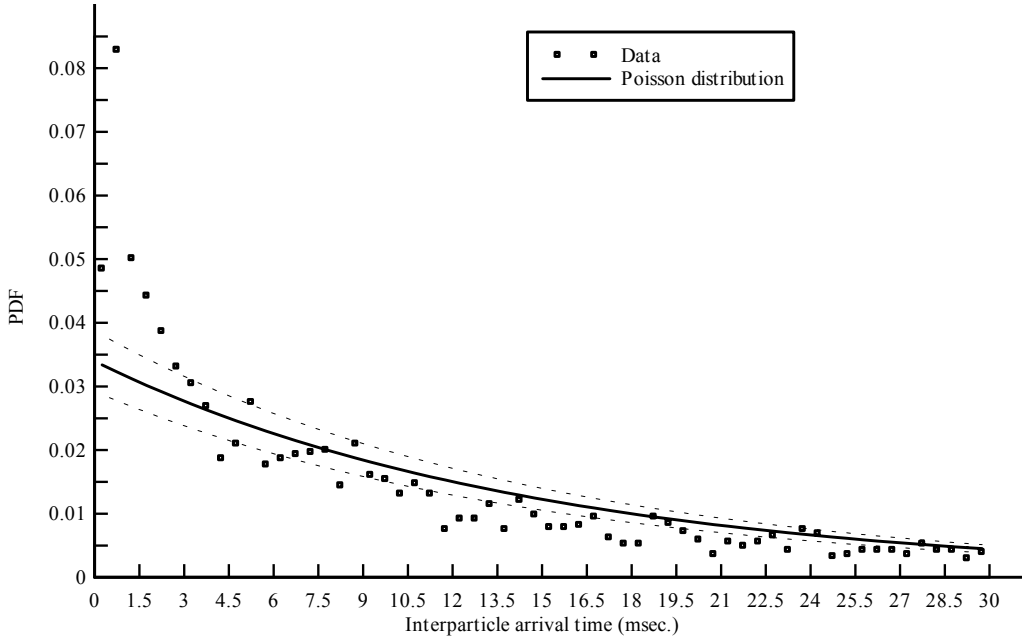

(A) Inter-particle arrival time distributions for bubble chord times between 0 and 0.5 msec., 3055 bubbles, $\chi^2 = 461$.

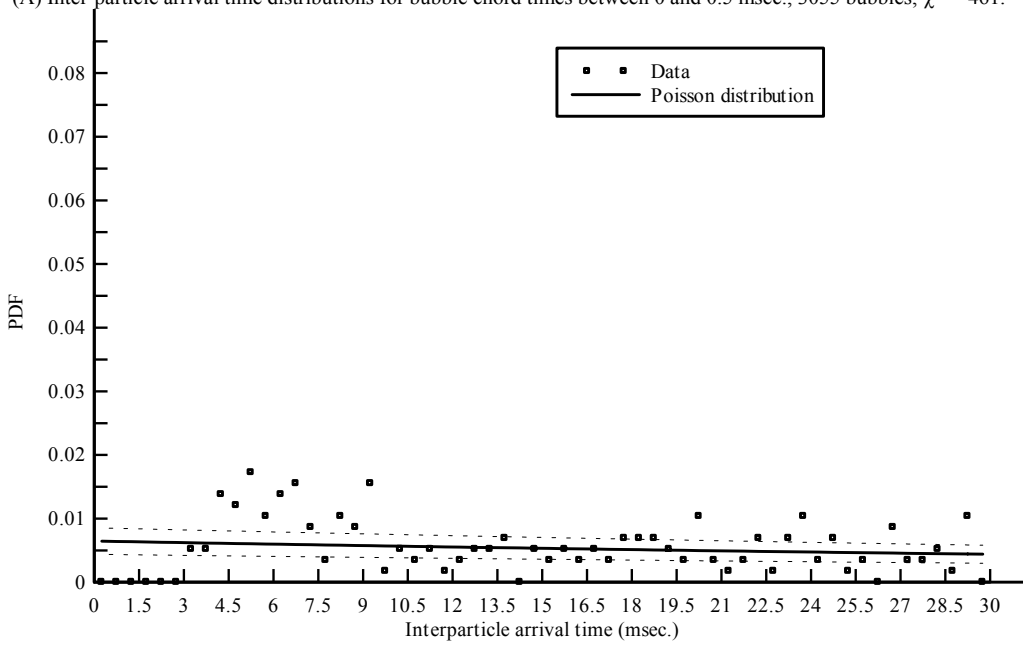

(B) Inter-particle arrival time distributions for bubble chord times between 3 and 5 msec., 581 bubbles, $\chi^2 = 110$.

Figure 7.15. Inter-particle arrival time distributions in the bubbly flow region of a hydraulic jump for different classes of air chord times - Comparison between data and Poisson distribution - Expected deviations from the Poisson distribution for each sample are shown in dashed lines - $Fr_1 = 8.5$, $\rho_w * V_1 * d_1 / \mu_w = 9.8$ E+4, $x\text{-}x_1 = 0.3$ m, $d_1 = 0.024$ m.

Altogether both approaches are complementary, although the inter-particle arrival time analysis may give some greater insight on the range of particle sizes affected by clustering.

7.5.2 Correlation analyses

When two or more phase detection probe sensors are simultaneously sampled, some correlation analyses may provide additional information on the bubbly flow structure. A well-known application is the use of dual tip probe to measure the interfacial velocity (Fig. 7.16). With large void fractions (C > 0.10), a cross-correlation analysis between the two probe sensors yields the time averaged velocity :

$$V = \frac{\Delta x}{T} \tag{36}$$

where T is the air-water interfacial travel time for which the cross-correlation function is maximum and Δx is the longitudinal distance between probe sensors (Fig. 7.16). Turbulence levels may be further derived from the relative width of the cross-correlation function :

$$Tu = 0.851 * \frac{\sqrt{\tau_{0.5}^2 - T_{0.5}^2}}{T} \tag{37}$$

where $\tau_{0.5}$ is the time scale for which the cross-correlation function is half of its maximum value such as: $R_{xy}(T+\tau_{0.5}) = 0.5*R_{xy}(T)$, R_{xy} is the normalised cross-correlation function, and $T_{0.5}$ is the characteristic time for which the normalised auto-correlation function equals : $R_{xx}(T_{0.5}) = 0.5$ (Fig. 7.16). Physically, a thin narrow cross-correlation function ($(\tau_{0.5}-T_{0.5})/T << 1$) must correspond to little fluctuations in the interfacial velocity, hence a small turbulence level Tu. While Equation (37) is not the true turbulence intensity u'/V, it is an expression of some turbulence level and average velocity fluctuations.

More generally, when two probe sensors are separated by a transverse or streamwise distance, their signals may be analysed in terms of the auto-correlation and cross-correlation functions R_{xx} and R_{xy} respectively. Figure 7.12B shows two probe sensors separated by a transverse distance Δz, while Figure 7.16 presents two probe sensors separated by a streamwise distance Δx. Practically the original data set may be segmented because the periodogram resolution is inversely proportional to the number of samples and it could be biased with large data sets (Hayes 1996).

Basic correlation analysis results include the maximum cross-correlation coefficient $(R_{xy})_{max}$, and the integral time scales T_{xx} and T_{xy} where :

$$T_{xx} = \int_{\tau=0}^{\tau=\tau(R_{xx}=0)} R_{xx}(\tau) * d\tau \tag{38}$$

$$T_{xy} = \int_{\tau=\tau(R_{xy}=(R_{xy})_{max})}^{\tau=\tau(R_{xy}=0)} R_{xy}(\tau) * d\tau \tag{39}$$

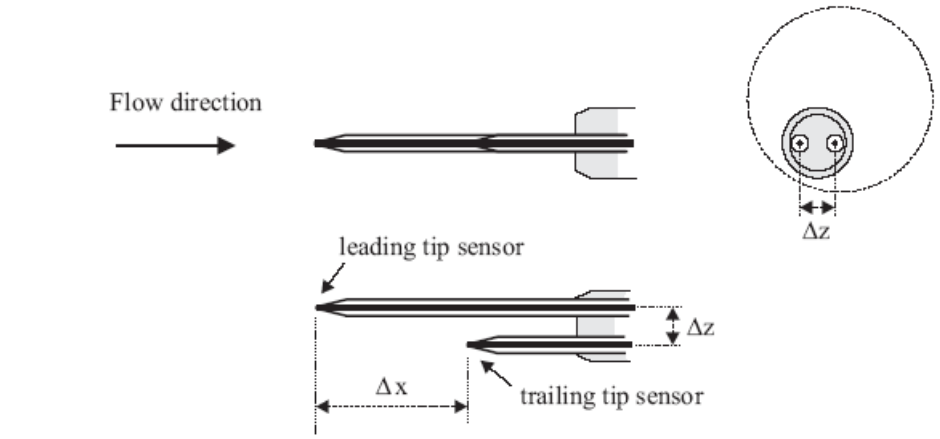

(A) Definition sketch.

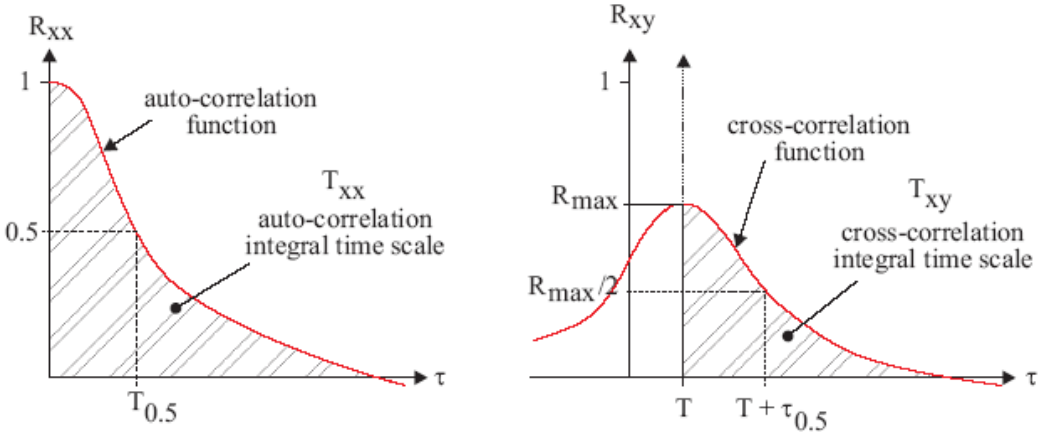

(B) Correlation functions.

Figure 7.16. Dual sensor phase detection probe.

where R_{xx} is the normalised auto-correlation function, τ is the time lag, and R_{xy} is the normalised cross-correlation function between the two probe output signals (Fig. 7.16). The auto-correlation integral time scale T_{xx} represents the integral time scale of the longitudinal bubbly flow structure. It is a characteristic time of the eddies advecting the air-water interfaces in the streamwise direction. The cross-correlation time scale T_{xy} is a characteristic time scale of the vortices with a length scale y advecting the air-water flow structures. The length scale y may be a transverse separation distance Δz or a streamwise separation Δx.

When identical experiments are repeated with different separation distances y (y = Δz or Δx), an integral turbulent length scale may be calculated as :

$$L_{xy} = \int_{y=0}^{y=y((R_{xy})_{max}=0)} (R_{xy})_{max} * dy \quad (40)$$

The length scale L_{xy} represents a measure of the transverse/streamwise length scale of the large vortical structures advecting air bubbles and air-water packets.

A turbulence integral time scale is :

$$T = \frac{\int_{y=0}^{y=y((R_{xy})_{max}=0)} (R_{xy})_{max} * T_{xy} * dy}{L_{xy}} \quad (41)$$

T represents the transverse/streamwise integral time scale of the large eddies advecting air bubbles.

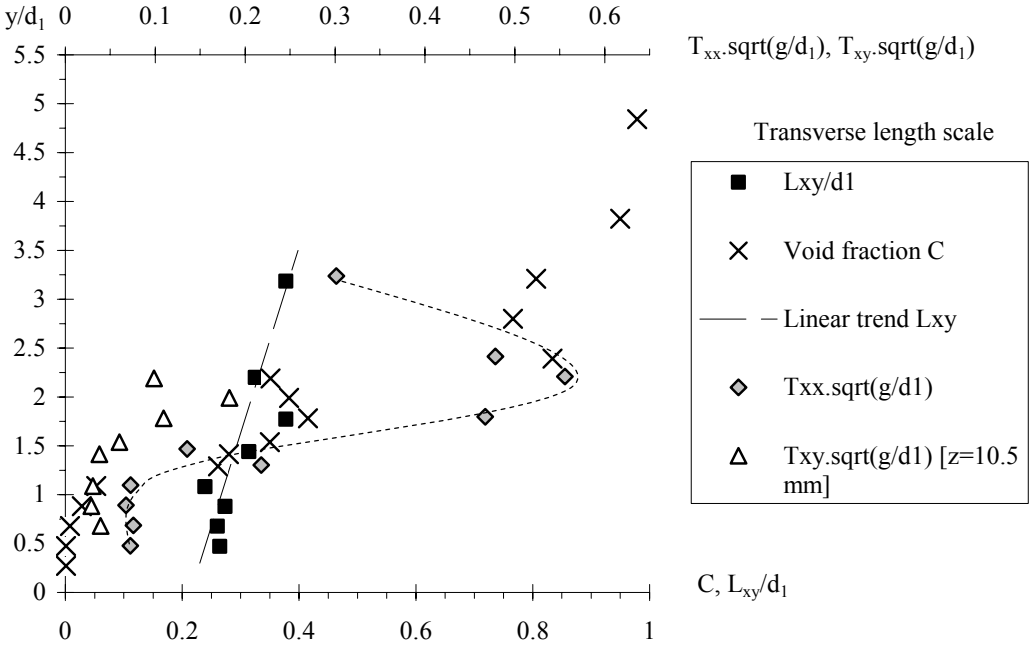

Figure 7.17. Dimensionless distributions of auto- and cross-correlation time scales $T_{xx}*\sqrt{g/d_1}$ and $T_{xy}*\sqrt{g/d_1}$ (transverse time scale, y = Δz = 10.5 mm), and transverse integral turbulent length scale L_{xy}/d_1 in a hydraulic jump - Fr_1 = 7.9, $\rho_w * V_1 * d_1/\mu_w$ = 9.4 E+4, x-x_1 = 0.1 m, d_1 = 0.0245 m.

Figures 17 to 19 present some experimental results obtained in a hydraulic jump on a horizontal channel and in a skimming flow on a stepped channel. In both flow situations, the distributions of integral time scales showed a marked peak for $0.4 \leq C \leq 0.6$ (Fig. 7.17 and 18). Note that Figure 7.17 presents some transverse time scales T_{xy} while Figure 7.18 shows some longitudinal time scales T_{xy}. The distributions of transverse integral length scales exhibited some marked differences that may reflect the differences in turbulent mixing and air bubble advection processes between hydraulic jump and skimming flows. In Figure 7.19, the integral turbulent length scale L_{xy} represents a measure of the transverse size of large vortical structures advecting air bubbles in the skimming flow regime. The air-water turbulent length scale is closely related to the characteristic air-water depth Y_{90} : i.e., $0.05 \leq L_{xy}/Y_{90} \leq 0.2$ (Fig. 7.19). Note that both the integral turbulent length and time scales were maximum for about C = 0.5 to 0.7 (Fig. 7.18 & 19). The finding emphasises the existence of large-scale turbulent structures in the intermediate zone ($0.3 < C < 0.7$) of the flow, and it is hypothesised that these large vortices may play a preponderant role in terms of turbulent dissipation.

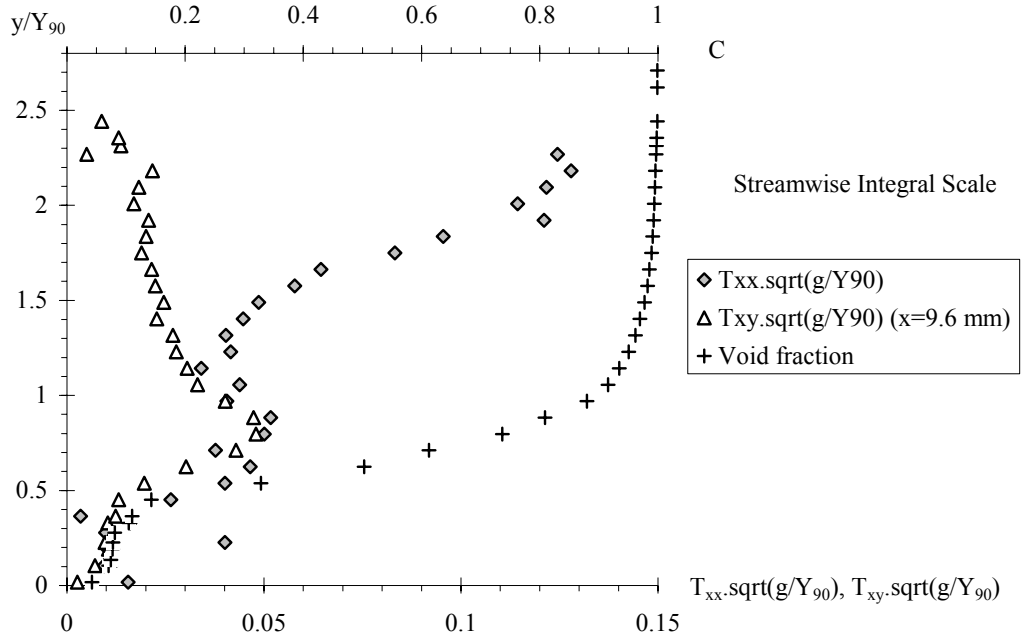

Figure 7.18. Dimensionless distributions of auto- and cross-correlation time scales $T_{xx}*\sqrt{g/Y_{90}}$ and $T_{xy}*\sqrt{g/Y_{90}}$ (longitudinal time scale, $y = \Delta x = 9.6$ mm) in a skimming flow on a stepped chute - $d_c/h = 1.15$, $\rho_w*V*d/\mu_w = 1.2$ E+5, Step 10, $Y_{90} = 0.0574$ m, $h = 0.1$ m, $\theta = 22°$.

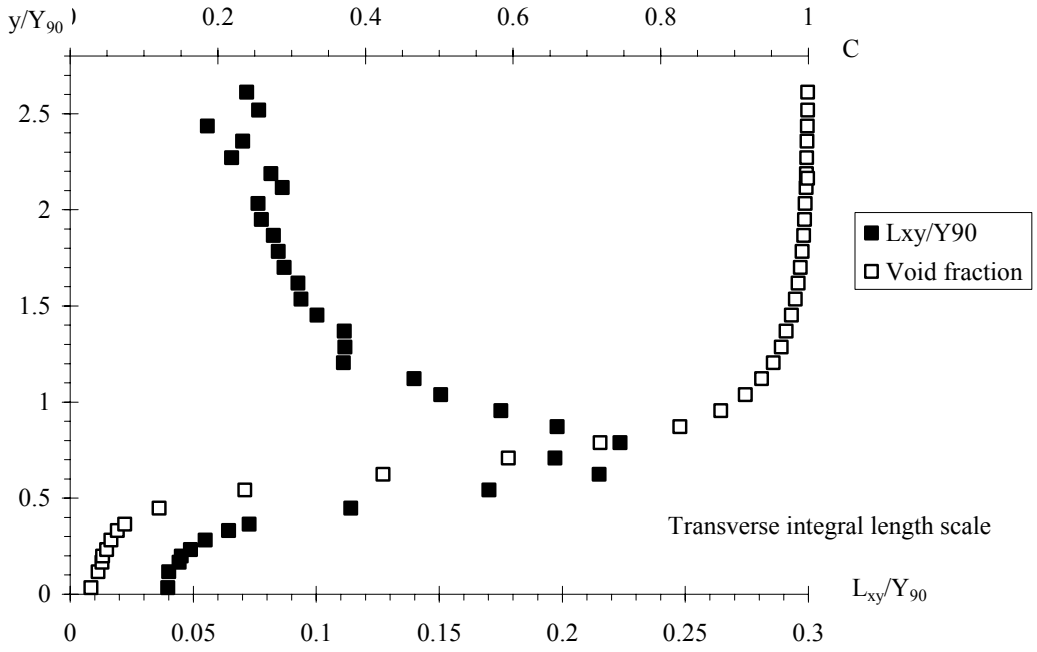

Figure 7.19. Dimensionless distributions of transverse integral turbulent length scale L_{xy}/Y_{90} in a skimming flow on a stepped chute - $d_c/h = 1.15$, $\rho_w*V*d/\mu_w = 1.2$ E+5, Step 10, $Y_{90} = 0.0598$ m, $h = 0.1$ m, $\theta = 22°$.

7.6 CONCLUDING REMARKS

In turbulent free-surface flows, the strong interactions between turbulent waters and the atmosphere may lead to some self-aeration. That is, the entrainment/entrapment of air bubbles that are advected within the bulk of the flow and give a 'white' appearance to the waters. In Nature, free-surface aerated flows are encountered at waterfalls, in mountain rivers and river rapids, and when wave breaking occurs on the ocean surface. 'White waters' provide always spectacular effects (Fig. 7.20). While classical examples include the tidal bore of the Qiantang river in China, the Zambesi rapids in Africa, and the 980 m high Angel Falls in South America, 'white waters' are observed also in smaller streams and torrents. The rushing waters may become gravitationless in waterfalls, impacting downstream on rocks and water pools where their impact is often surrounded by splashing, spray and fog (e.g. Niagara Falls). Man-made self-aeration is also common, ranging from artistic fountains to engineering and industrial applications.

The entrainment of air bubbles may be localised at a flow discontinuity or continuous along an air-water free-surface. At a flow singularity, air bubbles are entrained locally at the impinging point and they are advected in a region of high shear. Interfacial aeration is the air bubble entrainment process along an air-water interface that is parallel to the flow direction. A condition for the onset of air bubble entrainment may be expressed in terms of the tangential Reynolds stress and the fluid properties. With both singular and interfacial aeration, the void fraction distributions may be modelled by some analytical solutions of the advective diffusion equation for air bubbles.

The microscopic structure of turbulent bubbly flows is discussed based upon some developments in metrology and signal processing. The results may provide new information on the air-water flow structure and the turbulent eddies advecting the bubbles. However the interactions between entrained air bubbles and turbulence remain a key challenge for the 21st century researchers.

Figure 7.20. Dettifoss waterfall, Iceland (Courtesy of Paul Guard) - Fall height : 44 m, chute width : 100 m.

7.7 MATHEMATICAL AIDS

Definition	Expression	Remarks
Surface area of a spheroid (radii r1, r2)	$A = 2*p*r_1^2 + p*\frac{r_2^2}{\sqrt{1 - \frac{r_2^2}{r_1^2}}} * \mathrm{Ln}\left(\frac{1 + \sqrt{1 - \frac{r_2^2}{r_1^2}}}{1 - \sqrt{1 - \frac{r_2^2}{r_1^2}}}\right)$	r1 : equatorial radius, r2 : polar radius. Oblate spheroid (r1 > r2).
	$A = 2*p*r_1 * \left(r_1 + r_2 * \frac{\mathrm{Arcsin}\left(\sqrt{1 - \frac{r_1^2}{r_2^2}}\right)}{\sqrt{1 - \frac{r_1^1}{r_2^2}}}\right)$	Prolate spheroid (r1 < r2).
Bessel function of the first kind of order zero	$J_o(u) = 1 - \frac{u^2}{2^2} + \frac{u^4}{2^2 * 4^2} - \frac{u^6}{2^2 * 4^2 * 6^2} + \ldots$	also called modified Bessel function of the first kind of order zero
Bessel function of the first kind of order one	$J_1(u) = \frac{u}{2} - \frac{u^3}{2^2 * 4} + \frac{u^5}{2^2 * 4^2 * 6} - \frac{u^7}{2^2 * 4^2 * 6^2 * 8} + \ldots$	
Gaussian error function	$\mathrm{erf}(u) = \frac{2}{\sqrt{p}} * \int_0^u \exp(-t^2) * dt$	also called error function.

LIST OF SYMBOLS

List of Symbols		
Symbol	**Definition**	**Dimensions or Units**
A	bubble surface area	$[L^2]$
C	void fraction defined as the volume of air per unit volume	

	of air and water	
C_{mean}	depth-averaged void fraction	
D'	ratio of air bubble diffusion coefficient to rise velocity component normal to the flow direction time the characteristic transverse dimension of the shear flow	
D_t	air bubble turbulent diffusion coefficient	$[L^2 T^{-1}]$
D_0	dimensionless function of the void fraction	
$D^{\#}$	dimensionless air bubble turbulent diffusion coefficient	
F	air bubble count rate defined as the number of bubbles impacting the probe sensor per second	[Hz]
Fr_1	inflow Froude number of a hydraulic jump	
J_0	Bessel function of the first kind of order zero	
J_1	Bessel function of the first kind of order one	
K'	dimensionless integration constant	
L_{xy}	integral turbulent length scale	[L]
P	pressure	$[N L^{-2}]$
Q_{air}	entrained air flow rate	$[L^3 \cdot T^{-1}]$
Q_{water}	water discharge	$[L^3 \cdot T^{-1}]$
R_{xx}	normalized auto-correlation function	
R_{xy}	normalized cross-correlation function	
T	air-water interfacial travel time for which R_{xy} is maximum	[T]
T	transverse/streamwise turbulent integral time scale	[T]
$T_{0.5}$	characteristic time for which R_{xx}=0.5	[T]
T_{xx}	auto-correlation integral time scale	[T]
T_{xy}	cross-correlation integral time scale	[T]
Tu	turbulence intensity	
V_e	onset velocity for air entrainment	$[m s^{-1}]$
V_x	streamwise velocity	$[m s^{-1}]$
V_y	transverse velocity	$[m s^{-1}]$
V_1	jet impact velocity or inflow velocity in the hydraulic jump	$[m s^{-1}]$
$\vec{V}$	advective velocity vector	$[m s^{-1}]$
Y_{90}	characteristic distance where C = 0.90	[L]
d_{ab}	air bubble diameter	[L]
d_1	jet thickness at impact or inflow depth in hydraulic jump	[L]
erf	Gaussian error function	
g	gravitational acceleration constant	$[L T^{-2}]$
r	radius of sphere	[L]
r_1	radius of curvature of the free surface deformation	[L]
r_2	radius of curvature of the free surface deformation	[L]
r_1	equatorial radius of the ellipsoid	[L]
r_2	polar radius of the ellipsoid	[L]
t	time	[T]
$\overrightarrow{u_r}$	bubble rise velocity vector	$[m \cdot s^{-1}]$
u_r	bubble rise velocity	$[m \cdot s^{-1}]$
u_r	bubble rise velocity in a hydrostatic pressure gradient	$[m \cdot s^{-1}]$
v_i	turbulent velocity fluctuation in the streamwise direction	$[m \cdot s^{-1}]$
v_j	turbulent velocity fluctuation in the normal direction	$[m \cdot s^{-1}]$
x	longitudinal/streamwise direction	[L]

x_1	distance between the gate and the jump toe	[L]
y	transverse or radial direction	[L]
y'	dimensionless transverse or radial direction: $y' = y/Y_{90}$	
z	vertical direction positive upward	[L]
Δx	longitudinal distance between probe sensors	[L]
Δy	transverse distance between probe sensors	[L]
α_n	positive root for $J_0=(Y_{90}*\alpha_n)=0$	
θ	angle between the horizontal and the channel invert	
λ	dimensionless function of the mean air content	
μ_w	water dynamic viscosity	[M L^{-1} T^{-1}]
ρ_w	water density	[kg m^{-3}]
σ	surface tension between air and water	[N m^{-1}]
τ	time lag	[T]
$\tau_{0.5}$	time scale for which $R_{xy}=0.5*R_{xy}(T)$	[T]

REFERENCES

Brocchini, M., and Peregrine, D.H. (2001). "The Dynamics of Strong Turbulence at Free Surfaces. Part 1. Description." *Jl Fluid Mech.*, Vol. 449, pp. 225-254.

Cain, P. (1978). "Measurements within Self-Aerated Flow on a Large Spillway." *Ph.D. Thesis*, Ref. 78-18, Dept. of Civil Engrg., Univ. of Canterbury, Christchurch, New Zealand.

Carslaw, H.S., and Jaeger, J.C. (1959). "Conduction of Heat in Solids." *Oxford University Press*, London, UK, 2nd ed., 510 pages.

Chanson, H. (1988). "A Study of Air Entrainment and Aeration Devices on a Spillway Model." *Ph.D. thesis*, Ref. 88-8, Dept. of Civil Engrg., University of Canterbury, New Zealand.

Chanson, H. (1993). "Self-Aerated Flows on Chutes and Spillways." *Jl of Hyd. Engrg.*, ASCE, Vol. 119, No. 2, pp. 220-243. Discussion : Vol. 120, No. 6, pp. 778-782.

Chanson, H. (1997). "Air Bubble Entrainment in Free-Surface Turbulent Shear Flows." *Academic Press*, London, UK, 401 pages.

Comolet, R. (1979). "Vitesse d'Ascension d'une Bulle de Gaz Isolée dans un Liquide Peu Visqueux." ('The Terminal Velocity of a Gas Bubble in a Liquid of Very Low Viscosity.') *Jl de Mécanique Appliquée*, Vol. 3, No. 2, pp. 145-171 (in French).

Comolet, R. (1979). "Sur le Mouvement d'une bulle de gaz dans un liquide." ('Gas Bubble Motion in a Liquid Medium.') *Jl La Houille Blanche*, No. 1, pp. 31-42 (in French).

Crank, J. (1956). "The Mathematics of Diffusion." *Oxford University Press*, London, UK.

Cummings, P.D., and Chanson, H. (1999). "An Experimental Study of Individual Air Bubble Entrainment at a Planar Plunging Jet." *Chem. Eng. Research and Design*, Trans. IChemE, Part A, Vol. 77, No. A2, pp. 159-164.

Edwards, C.F., and Marx, K.D. (1995a). "Multipoint Statistical Structure of the Ideal Spray, Part I: Fundamental Concepts and the Realization Density." *Atomizati & Sprays*, Vol. 5, pp. 435-455.

Edwards, C.F., and Marx, K.D. (1995b). "Multipoint Statistical Structure of the Ideal Spray, Part II: Evaluating Steadiness using the Inter-particle Time Distribution." *Atomizati & Sprays*, Vol. 5, pp. 435-455.

Ervine, D.A., and Falvey, H.T. (1987). "Behaviour of Turbulent Water Jets in the Atmosphere and in Plunge Pools." *Proc. Instn Civ. Engrs., London*, Part 2, Mar. 1987, 83, pp. 295-314. Discussion: Part 2, Mar.-June 1988, 85, pp. 359-363.

Gonzalez, C.A. (2005). "An Experimental Study of Free-Surface Aeration on Embankment Stepped Chutes." *Ph.D. thesis*, Department of Civil Engineering, The University of Queensland, Brisbane, Australia, 240 pages.

Haberman, W.L., and Morton, R.K. (1954). "An Experimental Study of Bubbles Moving in Liquids." *Proceedings*, ASCE, 387, pp. 227-252.

Hayes, M.H. (1996). "Statistical, Digital Signal Processing and Modeling." *John Wiley*, New York, USA.

Hinze, J.O. (1955). "Fundamentals of the Hydrodynamic Mechanism of Splitting in Dispersion Processes." *Jl of AIChE*, Vol. 1, No. 3, pp. 289-295.

Murzyn, F., Mouaze, D., and Chaplin, J.R. (2005). "Optical Fibre Probe Measurements of Bubbly Flow in Hydraulic Jumps" *Intl Jl of Multiphase Flow*, Vol. 31, No. 1, pp. 141-154.

Toombes, L. (2002). "Experimental Study of Air-Water Flow Properties on Low-Gradient Stepped Cascades." *Ph.D. thesis*, Dept of Civil Engineering, The University of Queensland.

Wood, I.R. (1984). "Air Entrainment in High Speed Flows." *Proc. Intl. Symp. on Scale Effects in Modelling Hydraulic Structures*, IAHR, Esslingen, Germany, H. Kobus editor, paper 4.1.

Wood, I.R. (1991). "Air Entrainment in Free-Surface Flows." *IAHR Hydraulic Structures Design Manual No. 4*, Hydraulic Design Considerations, Balkema Publ., Rotterdam, The Netherlands, 149 pages.

Bibliography

Brattberg, T., and Chanson, H. (1998). "Air Entrapment and Air Bubble Dispersion at Two-Dimensional Plunging Water Jets." *Chemical Engineering Science*, Vol. 53, No. 24, Dec., pp. 4113-4127. Errata : 1999, Vol. 54, No. 12, p. 1925.

Brattberg, T., Chanson, H., and Toombes, L. (1998). "Experimental Investigations of Free-Surface Aeration in the Developing Flow of Two-Dimensional Water Jets." *Jl of Fluids Eng.*, Trans. ASME, Vol. 120, No. 4, pp. 738-744.

Brocchini, M., and Peregrine, D.H. (2001b). "The Dynamics of Strong Turbulence at Free Surfaces. Part 2. Free-surface Boundary Conditions." *Jl Fluid Mech.*, Vol. 449, pp. 255-290.

Carosi, G., and Chanson, H. (2006). "Air-Water Time and Length Scales in Skimming Flows on a Stepped Spillway. Application to the Spray Characterisation." *Report No. CH59/06*, Div. of Civil Engineering, The University of Queensland, Brisbane, Australia, July, 142 pages.

Cartellier, A., and Achard, J.L. (1991). "Local Phase Detection Probes in Fluid/Fluid Two-Phase Flows." *Rev. Sci. Instrum.*, Vol. 62, No. 2, pp. 279-303.

Chang, K.A., Lim, H.J., and Su, C.B. (2003). "Fiber Optic Reflectometer for Velocity and Fraction Ratio Measurements in Multiphase Flows." *Rev. Scientific Inst.*, Vol. 74, No. 7, pp. 3559-3565. Discussion & Closure: 2004, Vol. 75, No. 1, pp. 284-286.

Chanson, H. (1989). "Study of Air Entrainment and Aeration Devices." *Jl of Hyd. Res.*, IAHR, Vol. 27, No. 3, pp. 301-319.

Chanson, H. (2002a). "Air-Water Flow Measurements with Intrusive Phase-Detection Probes. Can we Improve their Interpretation ?." *Jl of Hyd. Engrg.*, ASCE, Vol. 128, No. 3, pp. 252-255.

Chanson, H,. (2002b). "An Experimental Study of Roman Dropshaft Operation : Hydraulics, Two-Phase Flow, Acoustics." *Report CH50/02*, Dept of Civil Eng., Univ. of Queensland, Brisbane, Australia, 99 pages.

Chanson, H. (2004a). "Environmental Hydraulics of Open Channel Flows." *Elsevier Butterworth-Heinemann*, Oxford, UK, 483 pages.

Chanson, H. (2004b). "Unsteady Air-Water Flow Measurements in Sudden Open Channel Flows." *Experiments in Fluids*, Vol. 37, No. 6, pp. 899-909.

Chanson, H. (2004). "Fiber Optic Reflectometer for Velocity and Fraction Ratio Measurements in Multiphase Flows. Letter to the Editor" *Rev. Scientific Inst.*, Vo. 75, No. 1, pp. 284-285.

Chanson, H. (2006). "Air Bubble Entrainment in Hydraulic Jumps. Similitude and Scale Effects." *Report No. CH57/05*, Dept. of Civil Engineering, The University of Queensland, Brisbane, Australia, Jan., 119 pages.

Chanson, H. (2007). "Bubbly Flow Structure in Hydraulic Jump." *European Journal of Mechanics B/Fluids*, Vol. 26, No. 3, pp. 367-384 (DOI:10.1016/j.euromechflu.2006.08.001).

Chanson, H. (2007). "Air Entrainment Processes in Rectangular Dropshafts at Large Flows." *Journal of Hydraulic Research*, IAHR, Vol. 45, No. 1, pp. 42-53.
Chanson, H., Aoki, S., and Hoque, A. (2006). "Bubble Entrainment and Dispersion in Plunging Jet Flows: Freshwater versus Seawater." *Jl of Coastal Research*, Vol. 22, No. 3, May, pp. 664-677.
Chanson, H., and Carosi, G. (2007). "Turbulent Time and Length Scale Measurements in High-Velocity Open Channel Flows." *Experiments in Fluids*, Vol. 42, No. 3, pp. 385-401 (DOI 10.1007/s00348-006-0246-2).
Chanson, H., and Manasseh, R. (2003). "Air Entrainment Processes in a Circular Plunging Jet. Void Fraction and Acoustic Measurements." *Jl of Fluids Eng.*, Trans. ASME, Vol. 125, No. 5, Sept., pp. 910-921.
Chanson, H., and Toombes, L. (2002). "Air-Water Flows down Stepped chutes : Turbulence and Flow Structure Observations." *Intl Jl of Multiphase Flow*, Vol. 28, No. 11, pp. 1737-1761.
Crowe, C., Sommerfield, M., and Tsuji, Y. (1998). "Multiphase Flows with Droplets and Particles." *CRC Press*, Boca Raton, USA, 471 pages.
Cummings, P.D. (1996). "Aeration due to Breaking Waves." *Ph.D. thesis*, Dept. of Civil Engrg., University of Queensland, Australia.
Cummings, P.D., and Chanson, H. (1997a). "Air Entrainment in the Developing Flow Region of Plunging Jets. Part 1 Theoretical Development." *Jl of Fluids Eng.*, Trans. ASME, Vol. 119, No. 3, pp. 597-602.
Cummings, P.D., and Chanson, H. (1997b). "Air Entrainment in the Developing Flow Region of Plunging Jets. Part 2 : Experimental." *Jl of Fluids Eng.*, Trans. ASME, Vol. 119, No. 3, pp. 603-608.
Gonzalez, C.A., and Chanson, H. (2004). "Interactions between Cavity Flow and Main Stream Skimming Flows: an Experimental Study." *Can Jl of Civ. Eng.*, Vol. 31.
Gonzalez, C.A., Takahashi, M., and Chanson, H. (2005). "Effects of Step Roughness in Skimming Flows: an Experimental Study." *Research Report No. CE160*, Dept. of Civil Engineering, The University of Queensland, Brisbane, Australia, July, 149 pages.
Heinlein, J., and Frtisching, U. (2006). "Droplet Clustering in Sprays." *Experiments in Fluids*, Vol. 40, No. 3, pp. 464-472.
Jones, O.C., and Delhaye, J.M. (1976). "Transient and Statistical Measurement Techniques for two-Phase Flows : a Critical Review." *Intl Jl of Multiphase Flow*, Vol. 3, pp. 89-116.
Luong, J.T.K., and Sojka, P.E. (1999). "Unsteadiness in Effervescent Sprays." *Atomization & Sprays*, Vol. 9, pp. 87-109.
Noymer, P.D. (2000). "The Use of Single-Point Measurements to Characterise Dynamic Behaviours in Spray." *Experiments in Fluids*, Vol. 29, pp. 228-237.
Straub, L.G., and Anderson, A.G. (1958). "Experiments on Self-Aerated Flow in Open Channels." *Jl of Hyd. Div.*, Proc. ASCE, Vol. 84, No. HY7, paper 1890, pp. 1890-1 to 1890-35.
Toombes, L., and Chanson, H. (2007). "Surface Waves and Roughness in Self-Aerated Supercritical Flow." *Environmental Fluid Mechanics*, Vol. 5, No. 3, pp. 259-270 (DOI 10.1007/s10652-007-9022-y).
Wood, I.R. (1983). "Uniform Region of Self-Aerated Flow." *Jl Hyd. Eng.*, ASCE, Vol. 109, No. 3, pp. 447-461.

Internet resources

Chanson, H. (2000). "Self-aeration on chute and stepped spillways - Air entrainment and flow aeration in open channel flows ." *Internet resource*.
(Internet address : http://www.uq.edu.au/~e2hchans/self_aer.html)
Chanson, H., and Manasseh, R. (2000). "Air Entrainment at a Circular Plunging Jet. Physical and Acoustic Characteristics - Internet Database." *Internet resource*.
(Internet address : http://www.uq.edu.au/~e2hchans/bubble/)

Cummings, P.D., and Chanson, H. (1997). "Air Entrainment in the Developing Flow Region of Plunging Jets. Extended Electronic Manuscript." *Jl of Fluids Engineering - Data Bank*, ASME (Electronic Files : 6,904 kBytes).
(Internet address : http://www.uq.edu.au/~e2hchans/data/jfe97.html)
Open access research reprints in air-water flows
(Internet address : http://espace.library.uq.edu.au/list.php?terms=chanson)
(Internet address : http://eprint.uq.edu.au/view/person/Chanson,_Hubert.html)

CHANSON, H. (2008). "Advective Diffusion of Air Bubbles in Turbulent Water Flows." in "Fluid Mechanics of Environmental Interfaces", *Taylor & Francis*, Leiden, The Netherlands, C. GUALTIERI and D.T. MIHAILOVIC Editors, Chapter 7, pp. 163-196 (34 pages) (ISBN 978-0-415-44669-3).